NOAA Technical Memorandum OAR ESRL-CSD-0001

doi:10.7289/V5X63JZV

Comparing near surface measurements of wind speed and direction over the Indian Ocean from Lidar and Scatterometer, and results from predictive study using the wind shear power law and the surface roughness log law to model upper level winds from near surface measurements.

Brandi J. McCarty
Brandi.McCarty@noaa.gov

Cooperative Institute for the Research in Environmental Sciences, CIRES
Boulder, CO

James H. Churnside
James.H.Churnside@noaa.gov

NOAA Earth System Research Laboratory
Boulder, CO

Earth System Research Laboratory
Chemical Sciences Division
325 Broadway
Boulder, CO 80305
April 2016

noaa NATIONAL OCEANIC AND ATMOSPHERIC ADMINISTRATION

Oceanic and Atmospheric Research Laboratories

Mention of a commercial company or product does not constitute an endorsement by NOAA. Use of information from this publication concerning proprietary products or the tests of such products for publicity or advertising purposes is not authorized.

Funding for this research has come from NASA (NNH13ZDA001N-WEATHER)

Contents

LIST OF FIGURES

LIST OF TABLES

LIST OF ABBREVIATIONS AND ACRONYMS

AMI ERS-1 Active Microwave Instrument

ASCAT Advanced SCATterometer

C-band 4-8 GHz portion of the electromagnetic spectrum

CMOD Model Function for C-Band Radar

CSD NOAA ESRL's Chemical Sciences Division

DYNAMO Dynamics of the Madden Julian Oscillation

ESRL NOAA Earth System Research Laboratory

EUMESAT European Organisation for the Exploitation of Meteorological Satellites

GMF Geophysical Model Function

HRDL High Resolution Doppler Lidar

ISRO Indian Space Research Organization

JPL NASA Jet Propulsion Laboratory

KNMI Royal Netherlands Meteorological Institute

Ku-band 12–18 GHz portion of the electromagnetic spectrum

MetOP-A EUMESAT satellite

NDBC National Data Buoy Center

NASA National Aeronautics and Space Administration

NOAA National Oceanic and Atmospheric Administration

NOIT National Institute of Ocean Technology

NRSC Normalized Radar Scattering Cross-section

NSCAT/NSCAT-2 NASA Scatterometers

NSCAT-4 OSCAT Geophysical Model Function

NWP SAF Numerical Weather Prediction Satellite Application Facility

Oceansat-2 ISRO Satellite

OSCAT Ocean Scatterometer-2

OSI SAF KNMI Ocean and Sea Ice Satellite Application Facility

PODACC NASA Jet Propulsion Laboratory Physical Oceanography Distributed Active Archive Center

PSD NOAA ESRL's Physical Sciences Division

QuikSCAT NASA Earth observation satellite, carried Seawinds scatterometer

RAMA Research Moored Array for African-Asian-Austrialian Monsoon Analysis and Prediction

SASS Seawinds Scatterometer on NASA QuikSCAT

TAO Tropical Atmosphere Ocean

TOGA NASA Tropical Ocean/Global Atmosphere

TRITON Triangle Trans-Ocean Buoy Network

LIST OF SYMBOLS AND VARIABLES

α Wind Shear Exponent

β Bias, estimated as mean difference

DOY Day Of Year 2011

m Slope

NRSC Normalized Radar Scattering Cross-section

N Number

ODR Orthogonal Direction Regression

Ri Richardson Number

RMS Root Mean Square

r Surface Roughness Length

SST Sea Surface Temperature

σ Standard Deviation

T_a Air Temperature

T_w Water Temperature

U_z Wind Speed at a height z

z Height in meters

Abstract

This study compares the equivalent neutral wind estimates of two space based active microwave sensors called scatterometers, the ASCAT (Advanced SCATterometer) and OSCAT (Oceansat-2 scatterometer), to the average wind profiles as estimated from continuous conical scans of a Doppler lidar deployed on a research vessel for a 3 month period in the Indian Ocean. Statistical analysis of matched pairs between the OSCAT derived wind speeds and the lidar measured wind speeds show the OSCAT is positively biased by 0.5 m s^{-1}. While the comparison between the pairs of lidar and ASCAT winds show no bias. The effect of atmospheric stability in estimating winds from surface roughness as compared to the Doppler wind measurements was investigated using a calculated stability indicator, Richardson number. Using the OSCAT and lidar matched pairs, analyses shows a statistical significant positive scatterometer bias (p-value < 0.01) of 0.83 m s^{-1} in wind speeds associated with unstable atmospheric conditions, or those with Richardson numbers greater than -0.4.

The vertical profiles of wind speed from the lidar not only capture winds near the surface, but also at heights up to 2 km. Data at between 50 m and 200 m is increasingly relevant as wind turbines for energy generation climb to these heights to harness more constant non-turbulent wind flow. Methods to model or extrapolate surface wind to upper levels exist. A wind shear power law or a surface roughness log law is commonly used by the wind energy industry. Using knowledge of atmospheric and surface conditions to constrain the shear exponent of the power law and surface roughness length of the log law, near surface wind speed estimates were extrapolated using these two models and compared to the lidar measured estimates at wind turbine heights. Biases between the modeled and lidar estimated winds found at rotor plane heights are presented. Using the log law and a surface roughness parameter of 0.01 to predict wind speeds at various heights and in 3 atmospheric stability scenarios, biases between the model and measurements range from 2.26 – 0.16 m s^{-1}.

1. Introduction

Since the JPL (*NASA Jet Propulsion Laboratory*) QuikSCAT (*SASS was the QuikSCAT scatterometer system*) was launched in 1978, space based scatterometers have provided global estimates of near surface wind speed and direction. Wind speed is inferred from the Normalized Radar Scattering Cross-section (NRSC), which is a function of surface roughness. Wind direction is inferred from the azimuthal dependence of the sea surface roughness relative to the wind direction. These wind products have been compared with other scatterometer, buoy, and dropwindsonde data, as well as, observations from research and voluntary observing vessels.

1.1 Scatterometer and Buoys

The utility of the first orbiting scatterometers, Seawinds and the NASA Scatterometers (NSCAT and NSCAT-2), has been established through comparisons with anemometers on buoys. Freilich and Dunbar (1999) used a nonlinear least squares fit between wind data from the U.S. National Data Buoy Center, NDBC, ocean buoys and the NSCAT and found a slope of 1.0, with residual root-mean square error of 1.3 m s^{-1}. Dickinson, Kelly et al. (2001) showed that the NSCAT-2 scatterometer derived winds compared well with the Tropical Atmosphere Ocean, TAO, buoy array in the Pacific Ocean, with zonal and meridional linear slopes of 0.97 and 1.01,

respectively. Plagge, Vandemark et al. (2009) shared results from linear regression analysis between co-located Seawinds scatterometer measurements and NDBC buoys in the Gulf of Maine where $speed_{QuikScat} = 0.96*(speed_{Buoy}) - 0.19$, and correlation coefficient, R, was 0.915. In the Indian Ocean, Satheesan, Sarkar et al. (2007) report mean differences in wind speed of 0.37 m s^{-1} and wind direction of 5.8° , and correlation coefficients of $R_{speed} = 0.87$ and $R_{dir} = 0.75$ for co-located Seawinds measurements with near surface wind measurements from moored National Institute of Ocean Technology (NIOT) buoys and a Triangle Trans-Ocean buoy Network (TRITON) buoy.

1.2 ASCAT and OSCAT and Buoys

The more recent scatterometers addressed in this paper have also been compared with winds from buoys. The Research Moored Array for African-Asian-Austrialian Monsoon Analysis and Prediction (RAMA) buoy wind estimates were compared to the satellite winds of the Oceansat-2 scatterometer, OSCAT, in the Indian Ocean by Rani and Gupta (2013). Co-located results from ~16 buoys show agreement, the monthly root mean square difference between OSCAT winds and buoy winds is 1.5-2.5 m s^{-1} and 8-15° for speed and direction, respectively. Monthly bias, calculated by subtracting buoy from OSCAT estimates, range from - 1.16 to 0.16 m s^{-1} for speed and -6.05 to 9.41° for direction.

Bentamy, Croize-Fillon et al. (2008) validated the European Meteorological Satellite Organization's Advanced SCATerometer (ASCAT) global wind estimates using NDBC buoy data. Using symmetrical regression analysis, a slope between 0.93 – 1.03 was reported depending on region. They also report wind speed from ASCAT is biased low by 0.5 m s^{-1}, with an RMS difference of 1.72 m s^{-1}. In the Bay of Bengal, Mahanty et al. report ASCAT has a small positive bias of 0.06 m s^{-1} with an RMSE of 0.96 and correlation coefficient of 0.95 when compared to NIOT buoys, (Mahanty 2012).

1.3 ASCAT and SASS and Dropwindsonde

ASCAT wind estimates have also been compared to the space based Seawinds scatterometer, SASS, as well as, to near surface dropwindsonde data deployed from aircraft. Symmetrical regression showed the slope of the best fit equation was 0.95, with a correlation coefficient of 0.94 m s^{-1} between satellite (ASCAT and SASS) instruments, Bentamy, Grodsky et al. (2012). They also suggest a bias in speed of up to 1 m s^{-1} in the tropical convergence zones, but no bias in wind direction. Chou, Wu et al. (2013) looked at the near surface wind estimates from Seawinds SASS and the averaged surface to 40 meter wind measurements from dropwindsonde and found 1.72 m s^{-1} and 18° RMS difference, in speed and direction respectively. A slight negative bias (ASCAT low) was determined for wind speeds less than 12 m s^{-1}, in speed of 1.7 m s^{-1}, and in direction of 23.3°.

1.4 Scatterometers and Research and Voluntary Vessels

Near surface wind observations are also available from research vessel platforms and have been compared to space based wind estimates. Co-located wind speed observations in the open ocean and the North Sea between the ERS-1 Active Microwave Instrument (AMI) and data from merchant ships were compared by Kent et al. (1998). Using a statistical model that accounted for error in both variables, they show the equation for the best fit was $speed_{ship} = 1.025*speed_{AMI} + 0.225$. Bourassa, Legler et al. (2003) report Seawinds validation by comparing the wind data to that of 8 research ships. Values vary by region (no comparison for Indian Ocean), but the global

RMS difference between Seawinds and research vessels for speed was 1.1 m s^{-1} and for direction = 15°. They also showed that the geophysical model function, GMF, used to estimate wind speed and direction from the backscatter coefficients produced slightly different bias, GMF^1 bias: speed = 0.06 m s^{-1}, direction = 1.6°, GMF^2 bias: speed = 0.01 m s^{-1}, direction = 1.99°.

2. Analysis of Lidar and Scatterometer Winds in Indian Ocean

The discussion in this article shows results from a comparison of the wind estimates from space based scatterometers, ASCAT and OSCAT, co-located with in situ wind measurements from a Doppler lidar aboard a research vessel in the Indian Ocean. Scatterometers estimate wind speed and direction using scatterometric backscatter measurements of surface roughness. Wind speed and direction are measured by scanning lidar using the Doppler shift technique and combining estimates from multiple scans to form vertical profiles.

The ASCAT and OSCAT instruments are active microwave sensors onboard two sun synchronous, polar orbiting satellites, EUMESAT (European Organisation for the Exploitation of Meteorological Satellites) MetOP-A and ISRO (Indian Space Research Organization) Oceansat-2, respectively. Not only is high resolution global data available at 12.5 km resolution from the scatterometers, but nearly daily co-located, spatially and temporally, data pairs between these scatterometers and the ship-based instruments, lidar and anemometer, are available for comparison.

2.1 Observation period and location

Over a 3 month period, 01-September-2011 to 06-December-2011, the DYNAMO, Dynamics of the Madden Julian Oscillation, experiment took place in the Indian Ocean. The Scripts Institution of Oceanography R/V Roger Revelle was deployed with NOAA Earth System Research Laboratory, ESRL, Doppler lidar and an air-sea flux package to retrieve the wind vector, as well as, air and sea surface temperature measurements. Figure 1 shows the region of interest and the comparison locations.

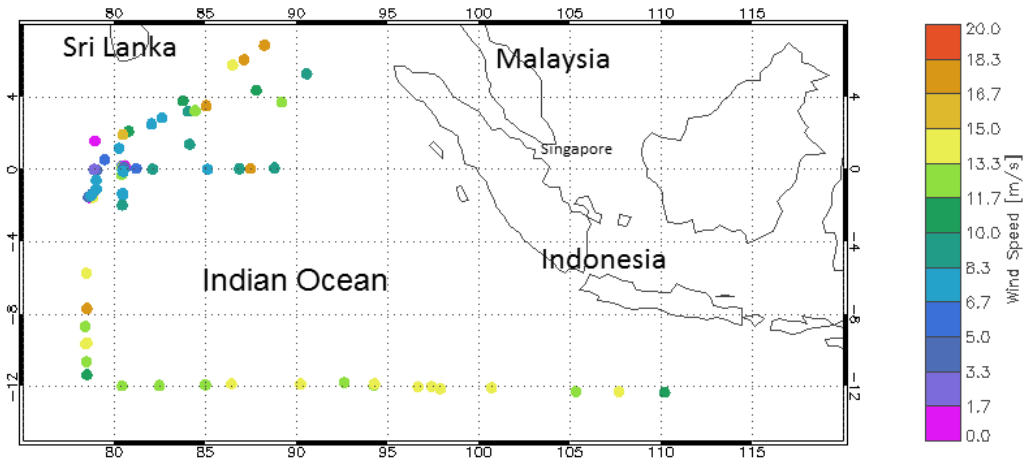

Figure 1. Location of the paired, ship based lidar and space based scatterometer, wind speed estimates along the R/V Roger Revelle ship track.

2.2 Advanced SCATterometer -- ASCAT

ASCAT is a C-Band, 5.25 GHz, dual pencil-beam rotating scatterometer. ASCAT uses six beams at three look angles, and provides backscattering cross-section measurements with two 550 km wide swaths separated by the satellite track (360 km). Three beams sweep the right side of the satellite ground track while three beams sweep the left. This allows the wind to be probed in multiple directions. These backscatter cross-section measurements paired with a geophysical inversion model are used to derive near surface (10 m) equivalent neutral wind speed. Additionally, the ASCAT signal response depends on the incident angle between the pulse and the ocean wave, this information is used to infer direction. The ASCAT mission required the wind speed and direction retrievals with accuracy of 2 m s^{-1} and 20°, respectively, over wind speeds of 4 – 24 m s^{-1}, Gelsthorpe, Schied et al. (2000), Figa-Saldana, Wilson et al. (2002), Wilson, Anderson et al. (2010), Verhoef and Stoffelen (2010).

Geophysical Model Functions (GMF) relate the backscatter, NRSC, from surface waves to surface stress indicating wind conditions. Using a GMF called CMOD for C-Band radar, estimates of equivalent neutral wind speed are derived from ASCAT data, Hersbach, Stoffelen et al. (2007), and Verhoef, Portabella et al. (2008). These estimates represent the wind at 10 m in height from the surface assuming the atmosphere is neutrally stratified. Verhoef, Portabella et al. (2008) report that the mean difference between neutral and true winds is +0.2 m s^{-1} for ASCAT.

The level 2 ASCAT wind products used in this study are 10 m equivalent neutral stability winds. The highest spatial resolution of 12.5 km gridded data was chosen as it is expected that this data resolves smaller scale wind features in greater detail than the other available 25 or 50 km wind products. The data were obtained from the website http://www.knmi.nl/scatterometer/ascat_osi_l2_prod/ The Royal Netherlands Meteorological Institute (KNMI) processes and hosts the global ASCAT data as a part of the EUMETSTAT Ocean and Sea Ice Satellite Application Facility (OSI SAF), a project by Meteo France, the Norwegian Meteorological Institute and the Danish Meteorological Institute. The processing software for the KNMI wind products is developed within the framework of the Numerical Weather Prediction Satellite Application Facility (NWP SAF) sponsored by EUMETSAT. References and detailed ASCAT data descriptions are found in www.knmi.nl/scatterometer/publications/pdf/ASCAT_Product_Manual.pdf , Verhoef and Stoffelen (2010).

2.3 Oceansat-2 Scatterometer - OSCAT

The OSCAT is a Ku-Band, scanning scatterometer. It employs two pencil beams that sweep the surface in a circular pattern at 20 rpm at 13.5 GHz collecting backscatter cross-section measurements, (Jaruwatanadilok, Stiles et al. 2014). Like the ASCAT data, these measurements, along with a geophysical inversion model, are used to derive equivalent neutral wind speed, and likewise uses the incident angle between the pulse and the ocean wave to infer direction. The OSCAT mission required the wind speed and direction retrievals from the backscatter cross-section data to have accuracy of 2 m s^{-1} and 20°, respectively, over wind speeds of 4 – 24 m s^{-1}. Additionally, OSCAT data products issued by the OSI SAF are characterized by a wind component RMS error smaller than 2 m s^{-1} and a bias of less than 0.5 m s^{-1} in wind speed.

The NSCAT-2 Ku-band GMF was used in the retrieval of wind speed and direction from the OSCAT backscatter cross-section data. A linear scaling was applied to better represent wind

speeds above 15 ms^{-1} to these retrievals and the results carry the GMF designation NSCAT-4. Wind speeds reported from OSCAT used in this discussion have been retrieved from geophysical model function, NSCAT-2 Ku-band GMF, and modified to reflect NSCAT-4 retrievals, Wentz and Smith (1999).

High resolution (12.5 km grid) near surface neutral stability wind products from OSCAT, were obtained from the NASA Jet Propulsion Laboratory's, PODAAC, Physical Oceanography Distributed Active Archive Center in Pasadena, CA at http://podaac.jpl.nasa.gov/dataset/OS2_OSCAT_LEVEL_2B_OWV_COMP_12_V2 , (SeaPAC 2013). The archive is provided as a service to the oceanographic and meteorological research communities_on behalf of the NASA/JPL QuikSCAT Project in collaboration with the ISRO. Documentation may be found at ftp://podaac.jpl.nasa.gov/OceanWinds/oceansat2/L2B/oscat/jpl/docs/

2.4 Ship Measurements: Doppler Lidar and Flux

NOAA ESRL Chemical Sciences Division's, CSD, scanning, coherent, and pulsed High Resolution Doppler Lidar, HRDL, near-IR signal scatters off of aerosol targets carried by the wind, using the Doppler-shifted frequency between the transmitted and reflected light to provide range resolved estimates of line of sight or radial velocity (Grund, Banta et al. 2001). This study makes use of vertically resolved profiles of horizontal wind speed and wind direction computed from the radial velocities retrieved from a 20 minute scan sequence, consisting of azimuthal and elevation scans. The theory of retrieving vertical profiles of horizontal wind velocity and wind direction from lidar signal is detailed in Browning and Wexler (1968). The processing algorithms implemented for lidar data used in this discussion are detailed in Banta, Pichugina et al. (2006) and Pichugina, Banta et al. (2011). Deployed on the R/V Roger Revelle, the lidar acquired data, using onboard compensation to account for platform motion, nearly continuously from 01-Sept-2011 to 06-Dec- The motion compensation system actively stabilizes the beam and allows for high precision measurements that are void of reference frame acceleration and motion due to ocean wave activity, thus the wind speed and direction retrievals are estimates of true wind, (Pichugina et al. 2012). Although the lidar vertical profiles are from ~12 m to ~ 2000 m, the data point at the lowest height of each profile, with a mean value of approximately 15.5 m ASL is used in this discussion. The data at this height represent an average over a horizontal area of mean radius of 335.9 m. Lidar vertical profiles are available by email request to the authors, images are at: http://www.esrl.noaa.gov/csd/groups/csd3/measurements/dynamo/

In addition to the lidar measurements, the NOAA ESRL Physical Sciences Division, PSD, Air-Sea Interaction group deployed (Fairall, White et al. 1997) sonic anemometers mounted on the R/V Roger Revelle forward mast that also measured wind speed and direction. Gill Solent anemometers were installed at 17.5 m ASL. The anemometer wind estimates are very highly correlated (R = 0.97, m = 1.01) with the lidar data. Additionally, aYSI 46040 thermistor affixed to a tygon tube was dragged from a boom about 4 m from the hull, floating at a depth of 5 cm below the ocean surface, provided seawater temperature data. A Vaisala HMP-35 thermometer measured air temperature. The wind vector and temperature data, made available from ESRL with a time resolution of 5 minutes at http://www.esrl.noaa.gov/psd/psd3/cruises/ were averaged to 20 minutes.

2.5 Comparison Analysis

The scatterometer data sets were searched for co-located pairs in the ship-borne lidar data set. Initial spatial search criteria were within 1° radial distance and within 6 hours in time. A summary of the temporal and spatial differences between the lidar and scatterometer matches for the 01-Sept-2011 to 06-Dec-2011 data set is in Table 1.

	ASCAT and lidar	OSCAT and lidar
Max Time Difference	4.1 hours	4.7 hours
Mean Time Difference	0.17 hours	1.9 hours
Max Spatial Difference	9.8 km	9.7 km
Mean Spatial Difference	0.97 km	1.4 km

Table 1. A Summary of the spatial and temporal differences between the lidar and scatterometer matching pairs.

To compare scatterometer and lidar retrievals of wind speed and direction, we used an Orthogonal Direction Regression, ODR, (Cantrell (2008), (Isobe, Feigelson et al. (1990). This method accounts for variability in both measurements. The differences between the slope, *m*, of the regressions and unity, were tested using the hypothesis H_0: m = 1. The bias, β, was estimated as the mean difference between lidar and scatterometer estimates, and the significance of these values was obtained by evaluating the p-values from Student's T-tests or T-means tests.

Wind speed data from the OSCAT and the lidar were matched spatially and temporally over the entire experiment period from 01-Sept-2011 to 06-Dec-2011. 89 matches were found, with 81 points having speeds greater than 2 m s^{-1}. ODR and mean difference (bias) analysis results are included in Table 2. Two-sided Students-T tests reveal a statistically significant ~0.5 m s^{-1} bias between the two instruments for all wind speeds and for those greater than 2 m s^{-1}.

Wind Speed **U**	Bias (m s^{-1})	2-sided T-test		Regression Fit Parameters	m=slope b=intercept	H_0:m=1	H_0:b=0	Corr. Coeff.
	β	$p\text{-val}_{bias}$	N	m	b	$p\text{-val}_m$	$p\text{-val}_b$	R
Lidar - OSCAT	-0.507	0.004	89	1.022	0.405	0.93	0.12	0.81
Lidar - OSCAT (gt 2 m s^{-1})	-0.55	0.04	81	0.9966	0.571	0.92	0.11	0.77
Lidar – OSCAT (no rain)	-0.099	0.58	26	0.793	-0.688	0.92	0.0003	0.78
Lidar – OSCAT (gt 2 m s^{-1}, no rain)	-0.229	0.234	20	0.76	0.867	0.91	9.24E-05	0.74
Lidar - ASCAT	-0.009	0.97	49	0.9452	0.271	0.96	0.05	0.94
Lidar - ASCAT (gt 2 m s^{-1})	-0.066	0.59	39	0.891	0.685	0.96	0.43	0.92
ASCAT - OSCAT	-0.38	1.67E-31	3634	0.988	0.451	0.99	0.987	0.73
ASCAT – OSCAT (gt 4 m s^{-1})	-0.24	1.27E-11	2344	1.124	-0.625	0.98	0.979	0.63

Table 2. Wind Speed, U, statistical analysis results comparing matching lidar and scatterometer pairs, and scatterometer and scatterometer pairs, found in northern Indian Ocean, 01-Sept-2011 to 06-Dec-2011, with the exception of the OSCAT and lidar no rain comparison results, the time period is 30-Sept-2011 to 06-Dec-2011.

Wind speed data from the OSCAT and the lidar were matched spatially and temporally over the shorter time period from 30-Sept-2011 to 06-Dec-2011. Results from statistical comparison are shown in Table 2. 62 matches were found, with 48 points having speeds greater than 2 m s^{-1}. Although there are fewer matching pairs, additional information was available for this time period. A TOGA (Tropical Ocean/Global Atmosphere) C-Band Doppler Radar provided additional data to characterize the existence of rain within a 25 km distance from the lidar and less than 30 minutes in time. The radar data were quality controlled using software and hand editing as needed, the resulting images were visibly inspected to determine the rain-free cases. While reducing the data set, 26 of the 62 matches were determined to be rain free, with 20 of these points having data greater or equal to 2 m s^{-1}. Using all the matched data over the shorter time period, (as well as, wind speed data greater than 2 m s^{-1}), a student's T-test, revealed that the computed OSCAT wind speeds have a statistically significant positive bias when compared to lidar wind speeds. After removing data points where rain was indicated within the larger 25 km TOGA footprint, the same analysis showed a smaller and statistically insignificant bias. Randomly reducing the "all data set" to a sample size of 26, (the number of samples with additional information about known rain), as well as the "greater than 2 m s^{-1} data set" revealed no statistical evidence that a the bias between the two instruments can be attributed to either rain or using wind speeds greater than 2 m s^{-1} in the analysis. The results show that OSCAT wind speeds in both the reduced (*in time to 30-Sept-2011 to 06-Dec-2011 and rain influenced data removal*) and expanded data sets have a positive bias of ~0.5 m s^{-1}. The results show that the OSCAT and lidar wind speeds are closer in agreement during this Indian Ocean experiment than the results from Rani and Gupta (2013) where the OSCAT winds were compared to buoy wind speed measurements during the 2011 monsoon season.

Temporally and spatially matched ASCAT and lidar data were also found for the same time period, 39 of the 49 matches were greater or equal to 2 m s^{-1}. The operational frequency of the ASCAT is 5.22 GHz, and therefore makes it less sensitive to rain, (Verhoef and Stoffelen 2010) than the Ku Band, however, the TOGA radar data was visually inspected to eliminate matches that may have rain influence outside of the lidar observing volume. Table 2 shows very good agreement between the ASCAT and lidar data, and the wind speed data from these two instruments have no statistically significant bias between them.

The data from the two scatterometers, ASCAT and OSCAT, were also searched and paired. A larger spatial area of the Indian Ocean was considered for identifying matches between the scatterometers, from 8 N to 16 S in latitude, and 120 E to 65 E in longitude. 3634 comparable wind speed data points were found. The distribution of the scatterometer wind speed estimates and results of the ODR fit are shown in Figure 2.

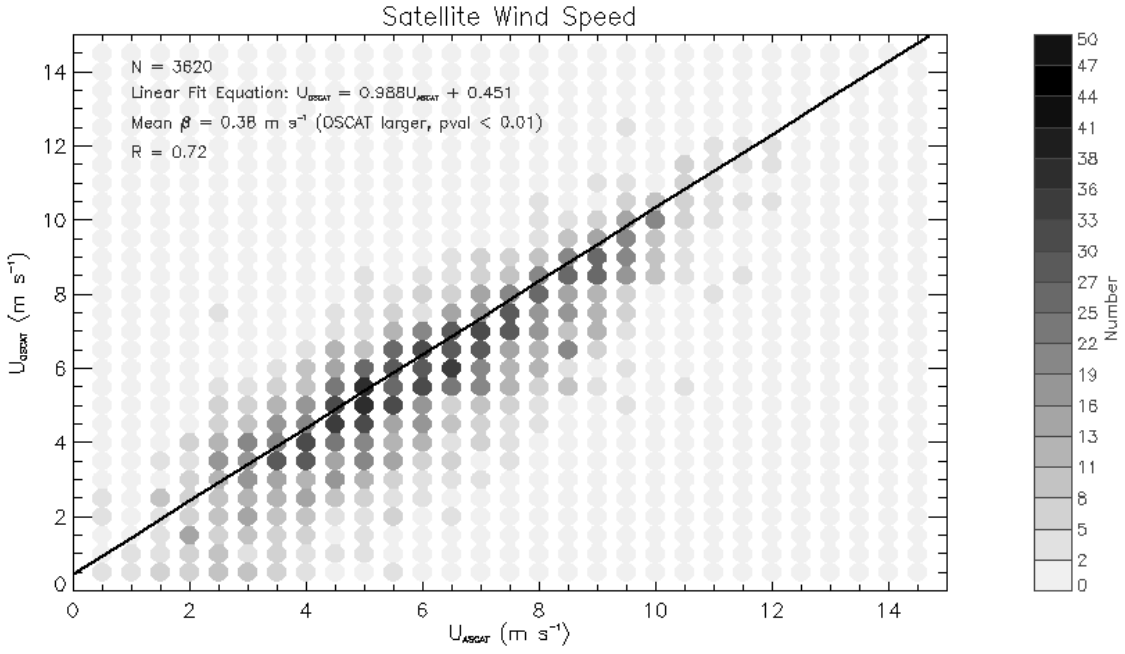

Figure 2. Wind Speed distribution from Scatterometer, U_{ASCAT} and U_{OSCAT}, and regression results for all matched pairs, 0 m s^{-1} ≤ U ≤ 20 m s^{-1}. Mean difference is U_{ASCAT} - U_{OSCAT}.

OSCAT wind speed estimates exhibit a statistically significant positive bias of 0.38 m s^{-1} when compared to the ASCAT estimates. Design specifications of the scatterometers indicate better skill in estimating wind speeds greater than 4 m s^{-1}, (Verhoef and Stoffelen 2009), with 2334 points meeting this speed threshold criteria, while the statistical analysis does not indicate results different than using all speeds, the bias of the OSCAT wind speed estimates of winds above 4 m s^{-1} does tighten slightly. Orthogonal Direction Regression results are listed in Table 2.

All three of these sensors not only provide wind speed estimates, but also estimate wind direction. Using the direction retrievals, at the same temporal and spatially matched wind speed locations as discussed previously, good statistical agreement is found between the sensors. The accuracy for the ASCAT and OSCAT wind direction retrievals is 20° over a wind speed range of 4 – 24 m s^{-1}. Using these parameters, and the knowledge that the OSCAT sensor's 13.5 Ghz operating frequency is more sensitive to rain contamination, Table 3 summarizes the statistical findings of the direction comparison. The distribution of the inferred wind direction from the all of the matched scatterometer-scatterometer pairs and fit results are shown in Figure 3. ODR resulted in the slope, m, in the best fit equation showing no statistical significance, while the offset, b, is. The bias, β, between these the wind direction estimates from the lidar and scatterometer comparisons are within the expected tolerance range of the scatterometer instrumentation, and not statistically significant.

Wind Direction	**Bias °N**	**2-sided T-test**		**ODR Fit Parameters**	**m=slope, b=intercept**	**H_0:m=1**	**H_0:b=0**
	β	**p-val$_{bias}$**	**N**	**m**	**b**	**p-val$_m$**	**p-val$_b$**
OSCAT – lidar	16.4	0.6	89	1.14	-27.5	0.95	5.45e-5
OSCAT - lidar (gt 2 m s^{-1})	1.18	0.77	81	1.04	-7.75	0.94	0.02
OSCAT - lidar (no rain)	-12.13	0.88	26	1.67	-160.38	0.9	0.0003
ASCAT – lidar	11.6	0.01	49	0.95	-8.27	0.91	0.0002
ASCAT - lidar (gt 2 m s^{-1})	-10.2	0.1	39	1.04	-17.9	0.93	0.02
ASCAT - OSCAT	-1	0.2	3634	1.1	-8.27	0.99	0.994
ASCAT - OSCAT (gt 4 m s^{-1})	-1.56	0.006	2344	1.02	-3.16	0.996	0.995

Table 3. Results of statistical analysis of wind direction estimates for 01-Sept-2011 to 06-Dec-2011, except the results reported for the "no rain" lidar and OSCAT comparison, it is 30-Sept-2011 to 06-Dec-2011.

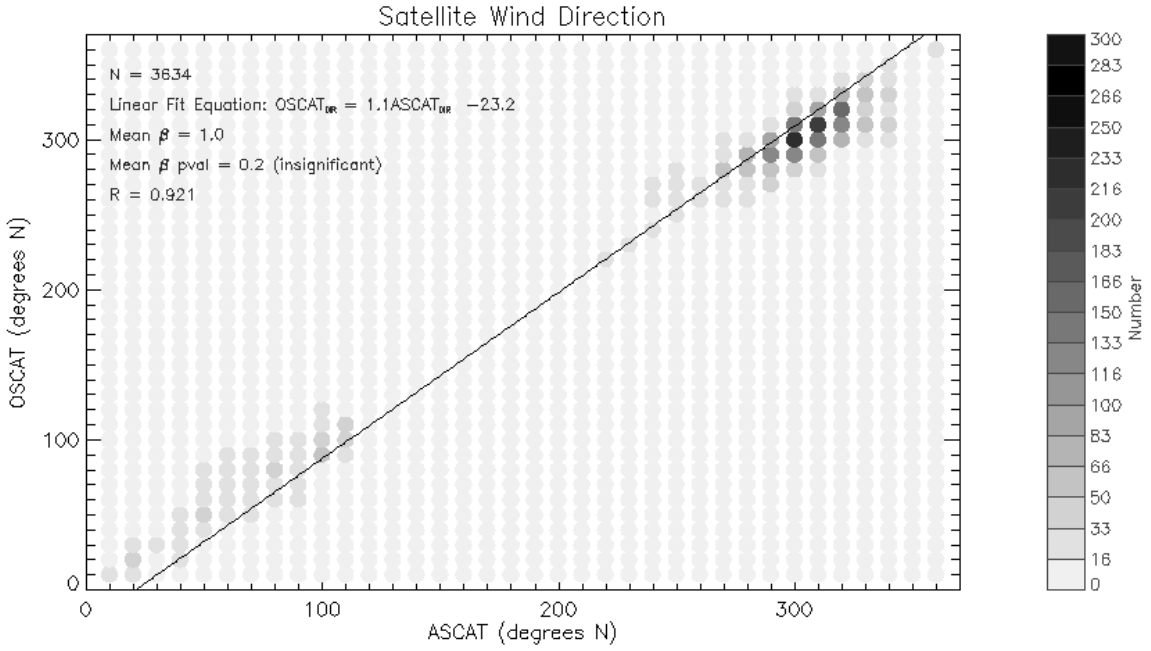

Figure 3. Inferred wind direction distribution and ODR results from scatterometer-scatterometer (ASCAT-OSCAT) comparison including direction corresponding to wind speeds, 0 m s^{-1} < U < 20 m s^{-1}.

2.6 Stability and Richardson Number

Successful wind retrievals from scatterometry depend on the effects of atmospheric stability and temperature remaining small compared to the surface roughness as detected by the backscattered signal. Kent (1998) showed that scatterometers were biased up to 30% due to increased stress at the surface in the North Sea. As an indicator of atmospheric stability, Richardson number, Ri, may be computed with measurements of air and sea surface temperatures, (Shaw and Churnside 1997).

$$Ri = \frac{g(T_a - T_w)z}{T_w U_z^2}, \qquad (1)$$

where g is gravitational acceleration, T_a and T_w are air and water temperatures (°C), z is the height of the wind measurement, and U_z is the measured wind speed at that height. This quantity is negative for unstable atmospheric conditions, zero for neutral, and positive for stable. Air and water temperatures were obtained from an instrument package specifically designed to measure air/sea fluxes, (Fairall, White et al. 1997), Zoumakis and Kelessis (1991).

Ri was computed; these estimates are found in Figure 4 for each of the lidar and scatterometer pairs, where the lidar wind speed was used in Equation 1. All Ri are negative in the 30-Sept-2011 to 06-Dec-2011 data set, with few positive values in the 01-Sept-2011 to 06-Dec-2011 data set. This indicates that the atmosphere was unstable to nearly neutral, and that sea surface temperatures were generally warmer than air temperatures for the matched observations. An unstable atmosphere favors turbulent vertical motions.

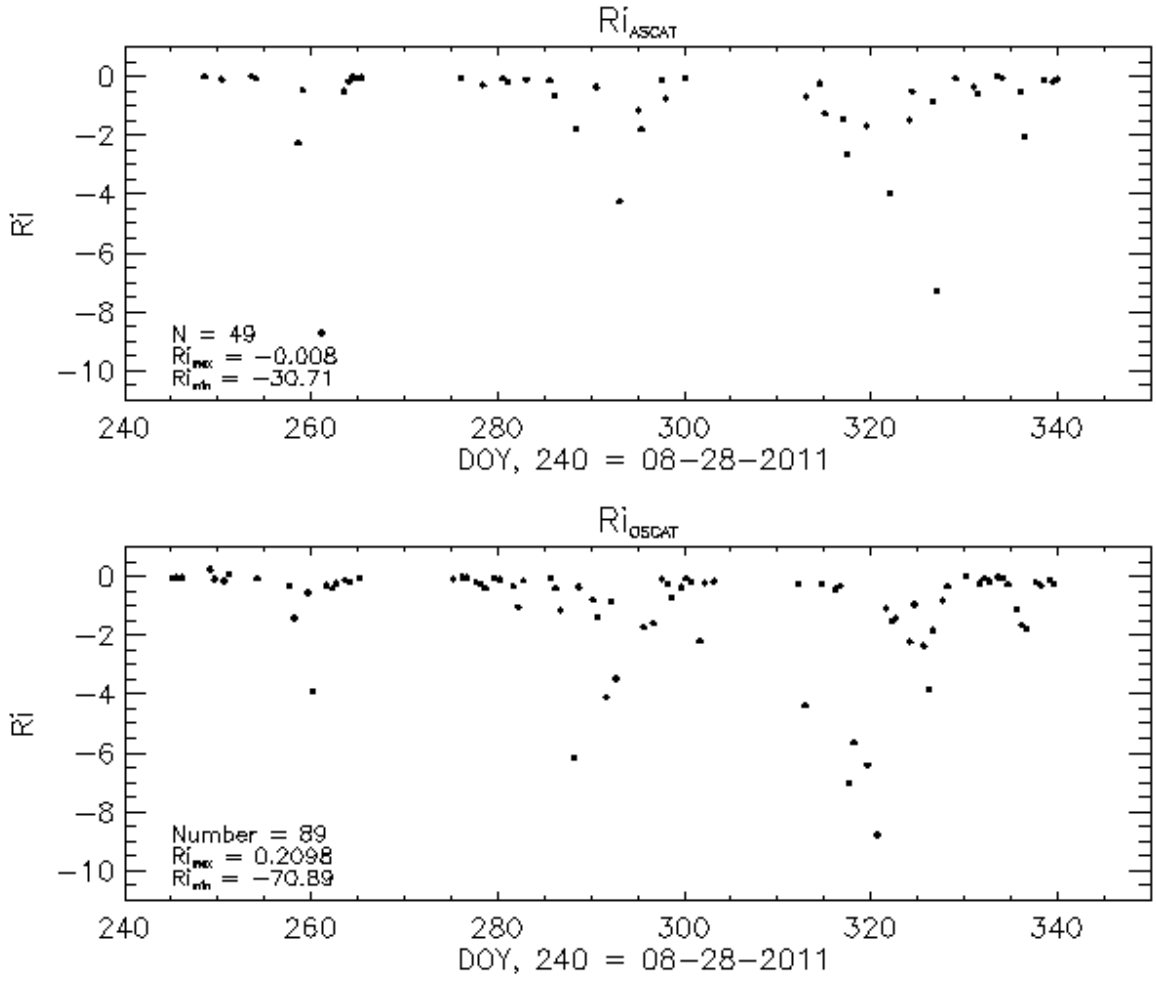

Figure 4. Richardson Number, Ri, using all matched lidar and the scatterometer pairs over 01-Sept-2011 to 06-Dec-2011. Top panel represents computed Ri with ASCAT wind speed, while the bottom panel are those computed with OSCAT wind speed. These lidar and scatterometer pairs were matched with SST and air temperature

from the NOAA ESRL PSD's Air-Sea Interaction Group measurements also on the R/V Roger Revelle in the northern Indian Ocean.

The measurement techniques differ between the lidar and scatterometer. Atmospheric stratification can cause equivalent neutral wind (scatterometer) to differ from Earth relative wind. The GMF techniques to infer wind speed from NRSC use an estimate of surface roughness in a neutrally stratified atmosphere. If vertical motion in the atmosphere is present, the sea surface roughness is expected to increase, creating the potential for the retrieval technique to overestimate wind speed.

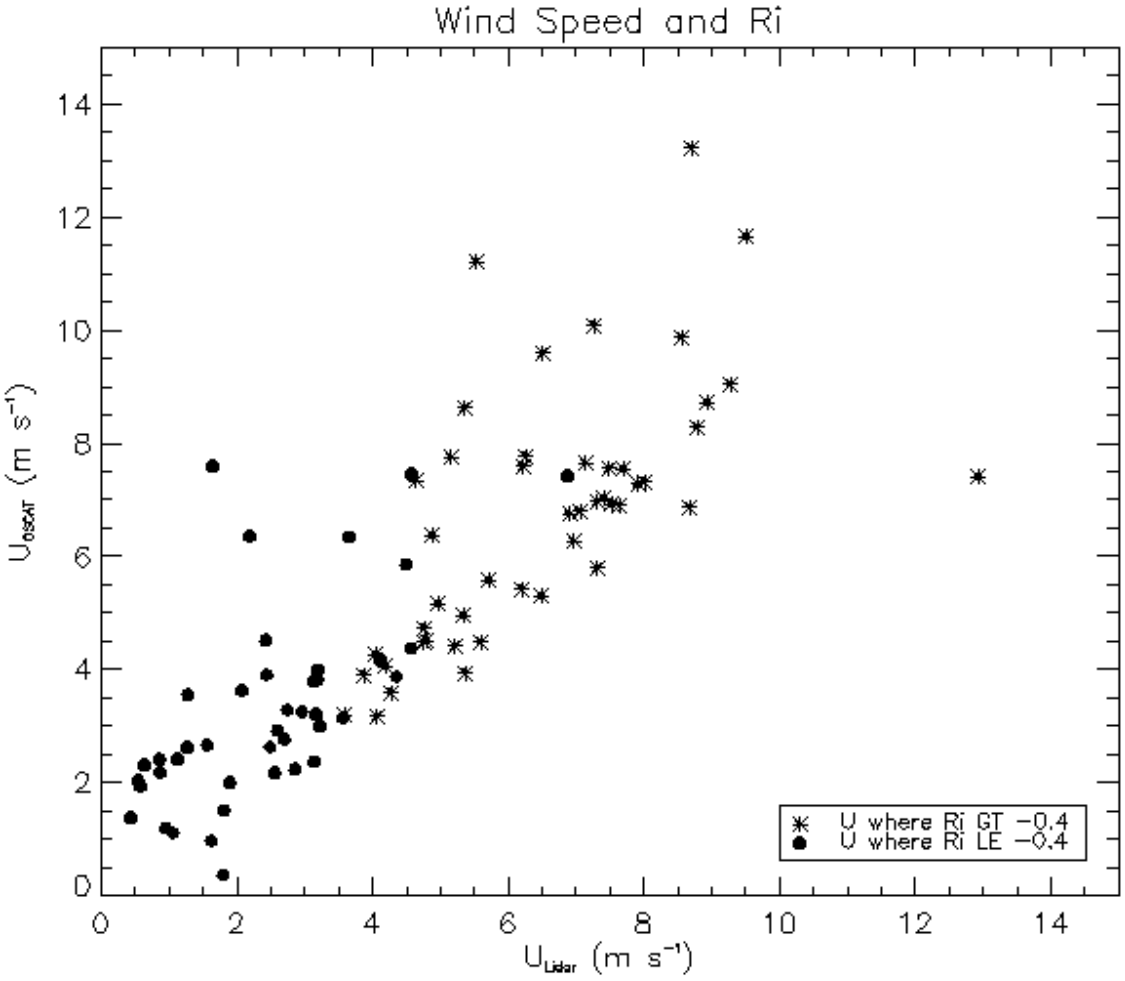

Figure 5. Lidar and scatterometer wind speed comparison with Richardson number, Ri, in symbols, using matched lidar and OSCAT pairs, 01-Sept-2011 to 06-Dec-2011. (No exclusions due to TOGA radar identified rain in larger observation region.) More unstable atmospheric conditions represented by circles, less unstable in stars.

The star symbols in Figure 5 demonstrate that nearly neutral atmospheric stability is characterized by wind speeds above ~4 m s^{-1}. Likewise, the light and variable winds below about 4 m s^{-1} (circles) are associated with instability in the atmosphere.

To determine if atmospheric stability plays a role in the 0.5 m s^{-1} bias seen between the lidar and the OSCAT wind speeds, a statistical comparison between the calculated Ri and the mean difference, β, in the two sensors wind speed estimates was done. The difference estimates and Ri

are pictured in Figure 6, and analysis results in Table 4. The wind speed measurements were apportioned in Ri with a threshold of -0.4, this value was chosen for an even number distribution in each part, with 47 speeds having associated Ri greater than -0.4, and 42 associated with less than -0.4. The results from this analysis show the more negative valued Ri, (more unstable atmospheric conditions), set of OSCAT wind speeds have a statistically significant positive bias when compared to the lidar wind speeds. Results are displayed in Table 4.

OSCAT	Lidar – Scatterometer Wind Speed ($m\ s^{-1}$) β	2-sided T-test p-val	Number N
U_{lidar} with Ri > -0.4	-0.22	0.41	47
U_{lidar} with Ri < -0.4	-0.83	0.0003	42

Table 4. Statistical results from a 2-sided Student's T-test between wind speed thresholded on -0.4 in Ri for $0\ m\ s^{-1} \leq U \leq 20\ m\ s^{-1}$.

The p-values for cases where all speeds, as well as those greater or equal to $2\ m\ s^{-1}$, indicate that atmospheric stability may be a factor in the OSCAT over estimating wind speeds. Using faster wind speeds in the analysis shows a slightly increased positive OSCAT bias, however is insignificant statistically, but represents only 51 of the original 89 matching pairs.

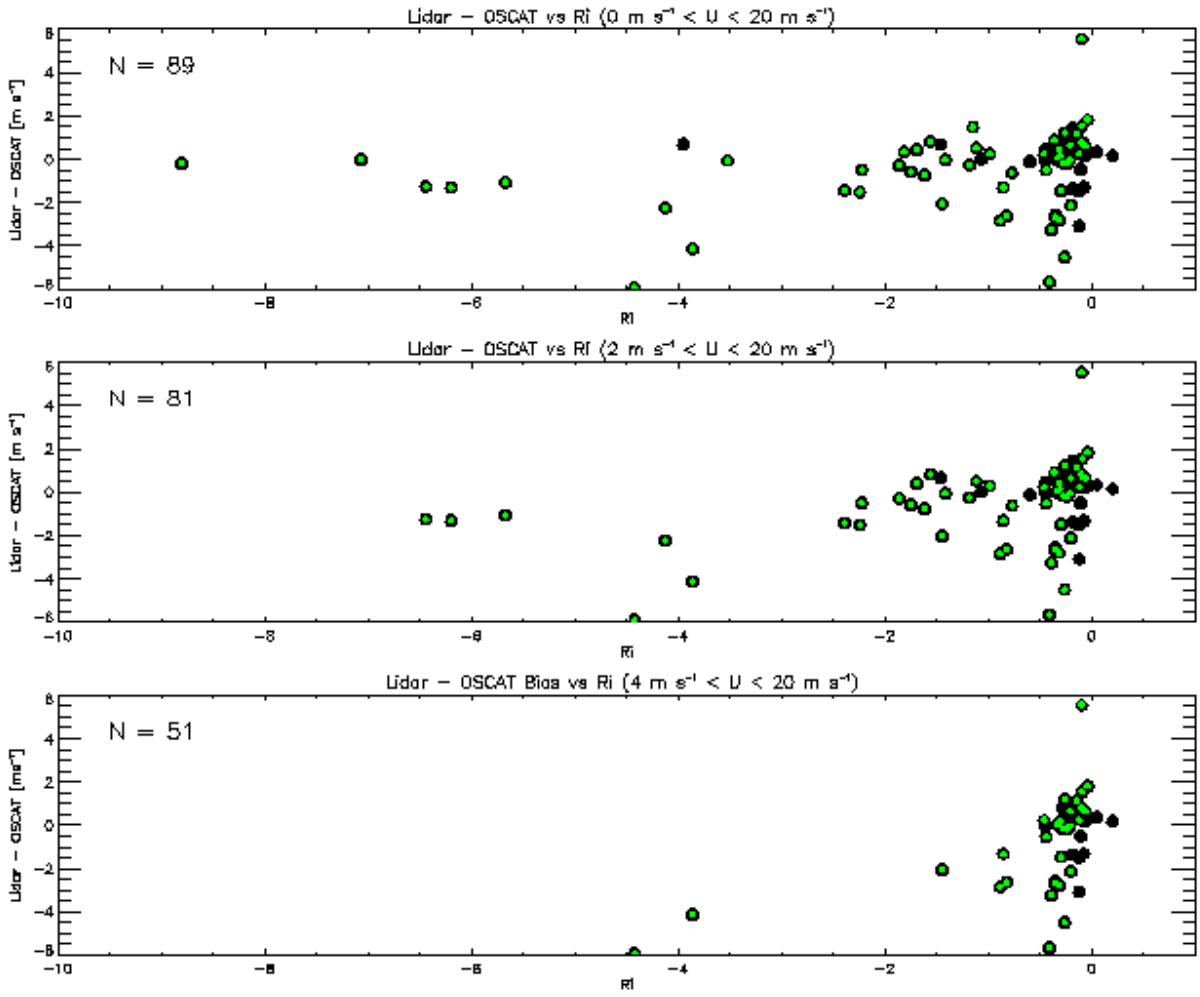

Figure 6. All Panels are Ri as a function of β_{OSCAT}, green points are rain-free identified with TOGA C-band radar image inspection, black represent all points. Top panel includes β_{OSCAT} from wind speed (0 m $s^{-1} \leq U \leq 20$ m s^{-1}), middle panel includes β_{OSCAT} from wind speeds (2 m $s^{-1} \leq U \leq 20$ m s^{-1}), bottom panel includes β_{OSCAT} from wind speeds (4 m $s^{-1} \leq U \leq 20$ m s^{-1}).

2.7 Findings

The temporal and spatial resolutions of the lidar and scatterometer wind speed and direction data vary, but matching pairs chosen on scales separated less than 6 hours in time, and 10 km in space agree well. The orthogonal regression implies better agreement between the ASCAT and lidar, with no statistically significant bias in wind speed or direction estimates, than with the OSCAT. The lidar and OSCAT regression results do point to a significant bias in wind speed of ~0.5 m s^{-1} using all estimated speed between 0 – 20 m s^{-1}. The p-value for the comparison of wind speeds using only speeds greater than 2 m s^{-1} and larger, p-value = 0.05, pointing to better agreement when eliminating the light and variable winds. Removing of any data potentially affected by rain, also shows little to no bias, and no significance, however, with only 26 points, the interpretation of the statistical test results are more fallacious.

The estimate of atmospheric stability, Ri, was computed; it was compared with the bias estimate between the lidar and the OSCAT. Although almost all matching lidar-scatterometer data pairs correspond to Ri indicating unstable to nearly neutral atmospheric situations, those with Ri < - 0.4 (most negative) do have statistically significance when compared to those with Ri > -0.4. The values of the wind speed associated with more negative Ri are also those light and variable speeds, less than ~4 m s^{-1}.

3. Upper Level Wind Estimation Using Near Surface Wind Measurements and Models

Energy generation from wind resources has emerged as an important part of a cleaner energy portfolio. Wind turbines are reaching heights of 100 – 200 m to harness the highest quality wind resource, yet the characterization and quantification of winds at these heights are largely unknown. Hasager, Pena et al. (2008) note the usefulness of SAR and scatterometer in wind estimates offshore. The number of samples from scatterometer is large, and they show good agreement with coastal meteorological observations.

Two methods are currently accepted in the wind energy community for modeling wind at upper levels using available near surface wind speed measurements, the wind shear power law and the log law, (Bratton 2011). Extrapolating wind speeds to turbine hub heights, as well as, the extent of the rotor plane, from surface measurements can yield poor results especially in atmospheric conditions that favor vertical motion. This study compares over 4200 vertical wind profiles from lidar, estimating wind speed near surface height (12.5 m), turbine hub height (100 m), rotor minimum (55 m) and maximum (155 m) heights, to modeled speeds using near surface data and the power and log law relationships. The data were collected in the northern Indian Ocean during a low activity cyclone year for the DYNAMO Experiment.

3.1 Wind Shear Power Law and Bias Results

The wind shear power law is used to predict wind speeds as they change with height. Based on a layer of fluid (air) flowing across a flat plate, Blasius predicted a shear exponent, α, in Equation 2, to be 1/7, Schlichting and Gersten (2000). While this α agrees with flat terrain, a value of 0.11 has been shown to better describe open water, (Bratton 2011). The wind shear power law is

$$U_2 / U_1 = (z_2 / z_1)^{\alpha} \qquad (2)$$

U_2 and U_1 are the wind speeds at heights z_2 and z_1 respectively, and α is the wind shear exponent.

The near surface wind speed data (12.5 m in height) were extracted from the vertical profiles retrieved by ship board lidar and used in Equation 2 to predict the values at 55, 100 and 155 m. The mean difference, β, between the model predicted values at these heights and the lidar observed values was calculated for two wind shear exponents, $\alpha = 0.1$ and $\alpha = 0.14$, commonly found in literature, (Bratton 2011). Results split into three atmospheric stability scenarios are found in Tables 5 and 6.

Wind Shear Power Law α= 0.1	z Height	Number	Mean Wind Speed Bias, β	σ
Atmospheric Stability	(m)		Lidar - model (m s^{-1})	
Very Unstable	55	389	-2.82	3.138
-100<Ri ≤-5	100	391	-2.44	2.591
	155	381	-1.36	1.681
Unstable	55	3228	-0.30	3.197
-5<Ri ≤-0.1	100	3305	-0.66	3.205
	155	3020	-0.85	2.075
Neutral	55	939	-0.30	3.263
-0.1<Ri ≤0.1	100	949	-0.66	2.858
	155	884	-0.85	1.582

Table 5. Estimated bias (mean difference) between measured and modeled wind speed. Measured near surface wind speed and shear exponent, α = 0.1 was used in these wind shear power law model results, (Eq 2). σ is the standard deviation in the bias estimate.

Wind Shear Power Law α= 0.14	z Height	Number	Mean Wind Speed Bias, β	σ
Atmospheric Stability	(m)		Lidar - model (m s^{-1})	
Very Unstable	55	389	-3.02	3.298
-100<Ri ≤-5	100	391	-2.71	2.791
	155	381	-1.59	1.841
Unstable	55	3228	-0.56	3.298
-5<Ri ≤-0.1	100	3305	-1.07	3.373
	155	3020	-1.36	2.268
Neutral	55	939	0.91	3.355
-0.1<Ri ≤0.1	100	949	0.05	2.992
	155	884	-1.76	1.689

Table 6. Estimated bias, β, between estimated and modeled wind speed. Measured near surface wind speeds and shear exponent, α = 0.14 was used in the wind shear power law model (Eq 2). σ is the standard deviation in the bias estimate.

3.2 Surface Roughness Log Law and Bias Results

The log law is another predictive relationship used by the wind energy community for estimating wind speed at turbine heights of interest. The log law uses a surface roughness parameter in addition to the surface wind speed. The log law is

$$U_2 / U_1 = ln(z_2/r) / ln(z_1/r) \qquad (3)$$

U_2 and U_1 are the wind speeds at heights z_2 and z_1 respectively, and r is surface roughness length.

Because of the flat ocean surface and lack of obstacles (buildings, forests etc.) interrupting the wind flow in open water environments, the results from predicting upper level wind using the log law agree closer with observations than those results from the wind shear power law. The mean differences between the log law predicted values of wind speed and the lidar observed speeds are in Table 7 for three atmospheric stability conditions, neutral, unstable and very unstable.

Surface Roughness Log Law r = 0.001	Height, z	Number	Mean Wind Speed Bias	σ
Atmospheric Stability	(m)		Lidar - model (m s^{-1})	
Very Unstable	55	389	-0.16	0.057
-100<Ri ≤-5	100	391	-0.23	0.091
	155	381	-0.28	0.120
Unstable	55	3228	-0.73	0.346
-5<Ri ≤-0.1	100	3305	-1.02	0.480
	155	3020	-1.20	0.555
Neutral	55	939	-1.33	0.324
-0.1<Ri ≤0.1	100	949	-1.87	0.432
	155	884	-2.26	0.471

Table 7. Estimated bias (mean difference) between measured and modeled wind speed. Measured near surface wind speed and surface roughness length, r = 0.001 was used in these surface roughness log law model results, (Eq 3). σ is the standard deviation in the bias estimate.

The predictive abilities of two upper level wind speed estimation models, the wind shear power law and the surface roughness log law, were investigated in the open water of the Indian Ocean. The atmospheric conditions over the course of the DYNAMO experiment were predominantly unstable or near neutral, with over 3000 observations where $-5 \leq Ri \leq 0.1$. The mean differences at all three upper level heights and three atmospheric conditions are negative, indicating over prediction when using the near surface measurements in models compared to observations at multiple heights.

4. Conclusions

Over the 3 month period, 49 co-located ASCAT and lidar observations were identified with mean temporal differences between observations of 10.2 minutes, and mean spatial differences of 0.97 km. Statistical analysis show very good agreement between the ASCAT and the lidar observations of wind speed and direction, and demonstrate no statistically significant bias between them.

Comparison of the 62 co-located OSCAT and lidar observations revealed a statistically significant positive OSCAT wind speed bias of 0.5 m s^{-1}. The location of the pairs of OSCAT and lidar observations is slightly greater both in time and in space than the ASCAT matches, differing by 1.4 km spatially and 1.9 hours temporally. Using Ri as an indicator of atmospheric stability, there is evidence that the positive wind speed bias the OSCAT sensor sees is associated with Ri < -0.4, or unstable atmospheric conditions.

Using a broader region of the northern Indian Ocean, 3634 co-located matches (0 m s^{-1} ≤ U ≤ 20 m s^{-1}) between the two scatterometer sensors (ASCAT and OSCAT) during the 3 month time period were identified. Regression results show good agreement with a slope of 0.988 and not statistically different than unity, and correlation coefficient, R = 0.72. Wind speeds retrieved by the OSCAT have a statistically significant positive bias of 0.24 m s^{-1} using speeds greater than the 4 m s^{-1} design specifications of the sensors. Wind direction inferred by the OSCAT also expresses a statistically significant bias, -1.56° N, p-value < 0.01. However, the direction estimates over all agree well with an R = 0.92 and slope result of 1.1 include all wind speeds 0 -20 m s^{-1}.

Continuous vertical wind speed profiles from Doppler lidar from the ship platform up to 1.5 km were available to compare with upper level wind speed predictions from models. Biases between the observations and the modeled predictions varied by height and as a function of atmospheric stability. The best model for the 01-Sept-2011 to 06-Dec-2011 time period in the open water of the northern Indian Ocean, using the lidar observations as truth, is the surface roughness log law model using a surface roughness length, r, of 0.001.

5. Acknowledgements

The authors would like to express a sincere thanks to the staff of the ESRL CSD Atmospheric Remote Sensing, ARS, group, including Alan Brewer, Ann Weickmann, Scott Sandberg, Raul Alvarez and Sara Tucker (formerly of the ARS group) for the deployment and attendance of the HRDL over the long experiment period, and post-processing of the lidar data. Thank you to Yelena Pichugina and Bob Banta for useful conversations related to atmospheric stability conditions, wind turbines and energy generation. The authors also appreciate the ESRL PSD Air-Sea Interaction group, including Chris Fairall, Sergio Pezoa, Ludovic Bariteau, and Dan Wolfe for collecting and processing the wind and temperature data and making it publicly accessible. Many thanks to the team at NASA Marshall Space Flight Center, including Timothy Lang, Xuanli Li, Kacie Hoover, Themis Chronis, Tyler Castillo for re-processing the TOGA C-Band Radar data and for the assistance in understanding models and many helpful conversations.

References

Banta, R. M., Y. L. Pichugina and W. A. Brewer (2006). "Turbulent Velocity-Variance Profiles in the Stable Boundary Layer Generated by a Nocturnal Low-Level Jet." Journal of the Atmospheric Sciences **63**(11): 2700-2719.

Bentamy, A., D. Croize-Fillon and C. Perigaud (2008). "Characterization of ASCAT measurements based on buoy and QuikSCAT wind vector observations." Ocean Sci. **4**(4): 265-274.

Bentamy, A., S. A. Grodsky, J. A. Carton, D. Croizé-Fillon and B. Chapron (2012). "Matching ASCAT and QuikSCAT winds." Journal of Geophysical Research: Oceans **117**(C2): C02011.

Bourassa, M. A., D. M. Legler, J. J. O'Brien and S. R. Smith (2003). "SeaWinds validation with research vessels." Journal of Geophysical Research: Oceans **108**(C2): n/a-n/a.

Bratton, D. C. W., C.A. (2011). The Wind Shear Exponent: Comparing Measured Against Simulated Values and Analyzing the Phenomena that Affect the Wind Shear. ASME 2011 5th International Conference on Energy Sustainability, Washington DC, The American Society of Mechanical Engineers.

Browning, K. A. and R. Wexler (1968). "The Determination of Kinematic Properties of a Wind Field Using Doppler Radar." Journal of Applied Meteorology **7**(1): 105-113.

Cantrell, C. A. (2008). "Technical Note: Review of methods for linear least-squares fitting of data and application to atmospheric chemistry problems." Atmospheric Chemistry and Physics **8**(17): 5477-5487.

Chou, K.-H., C.-C. Wu and S.-Z. Lin (2013). "Assessment of the ASCAT wind error characteristics by global dropwindsonde observations." Journal of Geophysical Research: Atmospheres **118**(16): 9011-9021.

Dickinson, S., K. A. Kelly, M. J. Caruso and M. J. McPhaden (2001). "Comparisons between the TAO Buoy and NASA Scatterometer Wind Vectors." Journal of Atmospheric and Oceanic Technology **18**(5): 799-806.

Fairall, C. W., A. B. White, J. B. Edson and J. E. Hare (1997). "Integrated Shipboard Measurements of the Marine Boundary Layer." Journal of Atmospheric and Oceanic Technology **14**(3): 338-359.

Figa-Saldana, J., J. J. W. Wilson, E. Attema, R. Gelsthorpe, M. R. Drinkwater and A. Stoffelen (2002). "The advanced scatterometer (ASCAT) on the meteorological operational (MetOp) platform: A follow on for European wind scatterometers." Canadian Journal of Remote Sensing **28**(3): 404-412.

Freilich, M. H. and R. S. Dunbar (1999). "The accuracy of the NSCAT 1 vector winds: Comparisons with National Data Buoy Center buoys." Journal of Geophysical Research: Oceans **104**(C5): 11231-11246.

Gelsthorpe, R., E. Schied and J. Wilson (2000). "ASCAT- Metop's advanced scatterometer." ESA bulletin **102**: 19-27.

Grund, C. J., R. M. Banta, J. L. George, J. N. Howell, M. J. Post, R. A. Richter and A. M. Weickmann (2001). "High-Resolution Doppler Lidar for Boundary Layer and Cloud Research." Journal of Atmospheric and Oceanic Technology **18**(3): 376-393.

Hasager, C. B., A. Pena, M. B. Christiansen, P. Astrup, M. Nielsen, F. Monaldo, D. Thompson and P. Nielsen (2008). "Remote Sensing Observation Used in Offshore Wind Energy." Selected Topics in Applied Earth Observations and Remote Sensing, IEEE Journal of **1**(1): 67-79.

Hersbach, H., A. Stoffelen and S. de Haan (2007). "An improved C-band scatterometer ocean geophysical model function: CMOD5." Journal of Geophysical Research: Oceans **112**(C3): C03006.
Isobe, T., E. D. Feigelson, M. G. Akritas and G. J. Babu (1990). "Linear-Regression in Astronomy .1." Astrophysical Journal **364**(1): 104-113.
Jaruwatanadilok, S., B. W. Stiles and A. G. Fore (2014). "Cross-Calibration Between QuikSCAT and Oceansat-2." Ieee Transactions on Geoscience and Remote Sensing **52**(10): 6197-6204.
Kent, E. C. (1998). "A comparison of ship- and scatterometer-derived wind speed data in open ocean and coastal areas." International Journal of Remote Sensing **19**(17): 3361-3381.
Mahanty, M. M., Muthiah, M. A., Latha, G. (2012). Comparison of ASCAT Derived Winds With In-Situ Buoy Measured Winds During Jal Cyclone. Pan Ocean Remote Sensing Conference. Kochi, Kerala, India, National Institute of Ocean Technology, Pallikaranai, Chennai, India. **11**.
Pichugina, Y. L., R. M. Banta, W. A. Brewer, S. P. Sandberg and R. M. Hardesty (2011). "Doppler Lidar–Based Wind-Profile Measurement System for Offshore Wind-Energy and Other Marine Boundary Layer Applications." Journal of Applied Meteorology and Climatology **51**(2): 327-349.
Plagge, A. M., D. C. Vandemark and D. G. Long (2009). "Coastal Validation of Ultra-high Resolution Wind Vector Retrieval From QuikSCAT in the Gulf of Maine." Geoscience and Remote Sensing Letters, IEEE **6**(3): 413-417.
Rani, S. and M. Gupta (2013). "Oceansat-2 and RAMA buoy winds: A comparison." Journal of Earth System Science **122**(6): 1571-1582.
Satheesan, K., A. Sarkar, A. Parekh, M. R. R. Kumar and Y. Kuroda (2007). "Comparison of wind data from QuikSCAT and buoys in the Indian Ocean." International Journal of Remote Sensing **28**(10): 2375-2382.
SeaPAC (2013). Oceansat-2 Scatterometer Level 2B Ocean Wind Vectors in 12.5 km Slice Composites Version 2. NASA Jet Propulsion Laboratory Physical Oceanography Distributed Active Archive Center. **2**.
Shaw, J. A. and J. H. Churnside (1997). "Scanning-laser glint measurements of sea-surface slope statistics." Applied Optics **36**(18): 4202-4213.
Verhoef, A., M. Portabella, A. Stoffelen and H. Hersbach (2008). CMOD5. n-the CMOD5 GMF for neutral winds, OSI SAF report, SAF/OSI/CDOP/KNMI/TEC/TN/165.
Verhoef, A. and A. Stoffelen (2009). "Validation of ASCAT 12.5-km winds." Ocean and Sea Ice SAF Technical Note SAF/OSI/CDOP/KNMI/TEC/RP/147.
Verhoef, A. and A. Stoffelen (2010). "ASCAT wind product user manual version 1.8." Report for the EUMETSAT OSI SAF.
Wentz, F. J. and D. K. Smith (1999). "A model function for the ocean-normalized radar cross section at 14 GHz derived from NSCAT observations." Journal of Geophysical Research: Oceans **104**(C5): 11499-11514.
Wilson, J. J. W., C. Anderson, M. A. Baker, H. Bonekamp, J. F. Saldana, R. G. Dyer, J. A. Lerch, G. Kayal, R. V. Gelsthorpe, M. A. Brown, E. Schied, S. Schutz-Munz, F. Rostan, E. W. Pritchard, N. G. Wright, D. King and U. Onel (2010). "Radiometric Calibration of the Advanced Wind Scatterometer Radar ASCAT Carried Onboard the METOP-A Satellite." Ieee Transactions on Geoscience and Remote Sensing **48**(8): 3236-3255.
Zoumakis, N. M. and A. G. Kelessis (1991). "The dependence of the bulk Richardson number on stability in the surface layer." Boundary-Layer Meteorology **57**(4): 407-414.